Mechanistic numerical modeling of solute uptake by plant roots

Andre Herman Freire Bezerra * Quirijn de Jong van Lier
Sjoerd E.A.T.M van der Zee Peter de Willingen

January, 2016

*Bezerra, A.H.F. and Q. de Jong van Lier, Exact Sciences Dep., ESALQ–Univ. of São Paulo, 13418-900 Piracicaba (SP), Brazil; S.E.A.T.M. van der Zee and P. Willingen, Dep. of Environmental Sciences, Wageningen Univ., Droevendaalsesteeg 4, 6708 PB Wageningen, the Netherlands.

Core ideas

- idea 1
- idea 2
- idea 3
- optional idea 4
- optional idea 5

Abstract

A modification in an existing water uptake and solute transport numerical model was implemented in order to allow the model to simulate solute uptake by the roots. The convection-dispersion equation (CDE) was solved numerically, using a complete implicit scheme, considering a transient state for water and solute fluxes and a soil solute concentration dependent boundary for the uptake at the root surface, based on the Michaelis-Menten (MM) equation. Additionally, a linear approximation was developed for the MM equation such that the CDE has a linear and a non-linear solution. A radial geometry was assumed, considering a single root with its surface acting as the uptake boundary and the outer boundary being the half distance between neighboring roots, a function of root density. The proposed solute transport model includes active and passive solute uptake and predicts solute concentration as a function of time and distance from the root surface. It also estimates the relative transpiration of the plant, on its turn directly affecting water and solute uptake and related to water and osmotic stress status of the plant. Performed simulations show that the linear and non-linear solutions result in significantly different solute uptake predictions when the soil solute concentration is below a limiting value (C_{lim}). This reduction in uptake at low concentrations may result in a further reduction in the relative transpiration. The contributions of active and passive uptake vary with parameters related to the ion species, the plant, the atmosphere and the soil hydraulic properties. The model showed a good agreement with an analytical model that uses a linear concentration dependent equation as boundary condition for uptake at the root surface. The advantage of the numerical model is it allows simulation of transient solute and water uptake and, therefore, can be used in a wider range of situations. Simulation with different scenarios and comparison with experimental results are needed to verify model performance and possibly suggest improvements.

Text

Crop growth is directly related to plant transpiration, and the closer the cumulative transpiration over a growing season is to its potential value, the higher will be the crop yield. Any stress occurring during crop development results in stomata closure and transpiration reduction, affecting productivity. Therefore, knowing how plants respond to abiotic stresses like those related to water and salt, and predicting and quantifying them, is important not only to improve the understanding of plant-soil interactions, but also to propose better crop management practices. The interpretation of experimental data to analyze the combined water and salt stress on transpiration and yield has been shown to be difficult due to the great range of possible interactions between the factors determining the behavior of the soil-plant-atmosphere (SPA) system. Modeling has been shown to be an elucidative manner to analyze the involved processes and mechanisms, providing insight in the interaction of water and salt stress.

Analytical models describing transport of nutrients in soil towards plant roots usually consider steady state conditions with respect to water flow to deal with the high non-linearity of soil hydraulic functions. Several simplifications (assumptions) are needed regarding the uptake of solutes by the roots, most of them also imposed by the non-linearity of the influx rate function. Consequently, although analytical models describe the processes involved in transport and uptake of solutes, they are only capable of simulating water and solute flow just for specific boundary conditions. Therefore, applying these models in situations that do not exactly correspond to their boundary condition may lead to a rough approximation but may also result in erroneous predictions. Many of the available analytical solutions include special math functions (Bessels, Airys or infinite series, for example) that need, at some point, numerical algorithms to compute results. For the case of the convection-diffusion equation, even the fully analytical solutions are restricted by numerical procedures, although with computationally efficient and reliable results.

As a substitute to analytical solutions, numerical modeling allows more flexibility when dealing with non-linear equations, being an alternative to better cope with diverse boundary conditions. The functions can be solved considering transient conditions for water and solute flow but with some pullbacks regarding numerical stability and more processing to perform calculations. In general, numerical models use empirical functions that relate osmotic stress to some electric conductivity of the soil solution. The parameters of these empirical models depend on soil, plant and atmospheric conditions in a range covered by the experiments used to generate data for model calibration. Using these models out of the measured range is not recommended and, in these cases, a new parameter calibration should be done. Physical/mechanistic models for the solute transport equations describe the involved processes in a wider range of situations since it is less dependent on experimental data, giving more reliable results.

In this study, we develop a mechanistic based numerical scheme to solve the convection-dispersion equation for radial root solute extraction. The model uses the water uptake scheme from De Jong van Lier et al. (2006). Assuming a boundary condition at root surface of concentration dependent solute uptake, the solution for the CDE considers transient flow of water and solute, as well as root competition. The model allows prediction of active and passive contributions to the solute uptake, which can be used to separate ionic and osmotic stresses by considering solute concentration inside the plant.

MATERIAL AND METHODS

Hydraulic Properties and Soil

Water uptake was analyzed using hydraulic data for three topsoils from the Dutch Staring series (Wösten et al., 2001) as listed in Table 1. The Van Genuchten (1980) equation system was used to describe K–θ–h relations for these soils:

$$\theta(h) = \theta_r + \frac{\theta_s - \theta_r}{[1 + |\alpha h|^n]^{1-(1/n)}} \tag{1}$$

$$K(\theta) = K_s \Theta^{\lambda} [1 - (1 - \Theta^{n/(n-1)})^{(1-(1/n))}]^2 \tag{2}$$

where θ ($m^3\ m^{-3}$) is the water content, K ($m\ s^{-1}$) and K_s ($m\ s^{-1}$) are respectively the hydraulic conductivity and the saturated hydraulic conductivity, h is the pressure head (m), Θ (–) is the effective saturation defined by $\frac{(\theta-\theta_r)}{(\theta_s-\theta_r)}$; θ_s ($m^3\ m^{-3}$) and θ_r ($m^3\ m^{-3}$) are the saturated and residual water contents, respectively; and α (m^{-1}), λ (–) and n (–) are empirical parameters.

Table 1: Soil hydraulic parameters used in simulations

Staring soil ID	**Textural class**	**Reference in this paper**	$\boldsymbol{\theta_r}$	$\boldsymbol{\theta_s}$	$\boldsymbol{\alpha}$	$\boldsymbol{\lambda}$	**n**	$\boldsymbol{K_s}$
			$m^3\ m^{-3}$		m^{-1}	–	–	$m\ d^{-1}$
B3	Loamy sand	Sand	0.02	0.46	1.44	-0.215	1.534	0.1542
B11	Heavy clay	Clay	0.01	0.59	1.95	-5.901	1.109	0.0453
B13	Sandy loam	Loam	0.01	0.42	0.84	-1.497	1.441	0.1298

Model Description

Microscopic root uptake models consider a single cylindrical root of radius r_0 (m) with an extraction zone being represented by a concentric cylinder of radius r_m (m) that bounds the half-distance between roots. The height of both cylinders is z (m) and represents the rooted soil depth. The basic assumptions of this type of model is that the root density does not change with depth and there is no difference in intensity of extraction along the root surface. Water and solute flows are axis-symmetric.

It is common to report root length density R ($m\ m^{-3}$) and r_0. These are related to r_m and root length L (m) by the following equations:

$$r_m = \frac{1}{\sqrt{\pi R}} \tag{3}$$

$$L = \frac{A_p z}{\pi {r_m}^2} \tag{4}$$

where A_p (m^2) is the soil surface area occupied by the plant. For the case that there is no available data from literature, one can obtain the value of L from relatively simple measurements of root and soil characteristics as soil mass (m_s, kg) and density (d_s, kg m^{-3}), and root average radius ($\overline{r_0}$, m) and R by

$$R = \frac{1}{\pi {r_m}^2} \,. \tag{5}$$

The geometry of the soil-root system considers an uniformly distributed parallel cylindrical root of radius r_0 and length z. To each root, a concentric cylinder of radius r_m and length z can be assigned to represent its extraction volume (Figure 1).

The discretization needed for the numerical solution was performed at the single root scale. As the extraction properties of the root are considered uniform along its length, and assuming no vertical differences in root density and fluxes, the cylinder can be represented by its cross-section, a circle. The area of this circle, representing the extraction region, was subdivided into n circular segments of variable size Δr (m), small near the root and increasing with distance, according to the equation De Jong van Lier et al. (2009):

$$\Delta r = \Delta r_{min} + (\Delta r_{max} - \Delta r_{min}) \left(\frac{r - r_0}{r_m - r_0} \right)^S \tag{6}$$

where the subscripts in Δr indicate the minimum and maximum segment sizes defined by the user, and S gives the rate at which the segment size increases. The parameter r_0 (m) represents the root radius, and r_m (m) is the radius of the root extraction zone, equal to the half-distance between roots, which relates to the root density R (m m^{-3}) according to Equation 3. This variable size discretization has the advantage to result in smaller segments in regions that need more detail in the calculations (near the root soil interface) due to the greater variation of expected fluxes. Figure 2 shows a schematic representation of the discretization as projected by Equation 6.

A fully implicit numerical treatment was given to the water and solute balance equations **??** and **??**. The Richards equation **??** for one-dimensional axis-symmetric flow can be written as

$$\frac{\partial \theta}{\partial t} = \frac{\partial \theta}{\partial H} \frac{\partial H}{\partial t} = C_w(H) \frac{\partial H}{\partial t} = \frac{1}{r} \frac{\partial}{\partial r} \left(r K(h) \frac{\partial H}{\partial r} \right) \tag{7}$$

where the total hydraulic head (H) is the sum of pressure (h) and osmotic (h_π) heads and C_w (m^{-1}) is the differential water capacity $\dfrac{\partial H}{\partial \theta}$. Relations between K, θ and h are described by the Van Genuchten (1980) equation system (Equations 1 and 2). Analogous to Van Dam and Feddes (2000), Equation 7 can be solved using an implicit scheme of finite differences with the Picard iterative process:

$$\begin{gathered} {C_w}_i^{j+1,p-1}(H_i^{j+1,p} - H_i^{j+1,p-1}) + \theta_i^{j+1,p-1} - \theta_i^j = \frac{t^{j+1} - t^j}{r_i \Delta r_i} \times \\ \left[r_{i-1/2} K_{i-1/2}^j \frac{H_{i-1}^{j+1,p} - H_i^{j+1,p}}{r_i - r_{i-1}} - r_{i+1/2} K_{i+1/2}^j \frac{H_i^{j+1,p} - H_{i+1}^{j+1,p}}{r_{i+1} - r_i} \right] \end{gathered} \tag{8}$$

where i ($1 \leq i \leq n$) refers to the segment number, j is the time step and p the iteration level. The Picard's method is used to reduce inaccuracies in the implicit numerical solution for the h-based Equation 7 Celia et al. (1990).

The solution for Equation 8 results in prediction of pressure head in soil as a function of time and distance from the root surface. The boundary conditions considered relate the flux density entering the root to the transpiration rate for the inner segment; and considers zero flux for the outer segment:

$$K(h) \frac{\partial h}{\partial r} = q = 0 \,, \qquad r = r_m \tag{9}$$

$$K(h) \frac{\partial h}{\partial r} = q_0 = \frac{T_p}{2 \pi r_0 R z} \,, \qquad r = r_0 \tag{10}$$

The computer algorithm that solves the Equation 8 and applies boundary conditions 9 and 10 can be found in Appendix **??**.

The convection-dispersion equation **??** for one-dimensional axis-symmetric flow can be written as

$$r\frac{\partial(\theta C)}{\partial t} = -\frac{\partial}{\partial r}\left(rqC\right) + \frac{\partial}{\partial r}\left(rD\frac{\partial C}{\partial r}\right). \tag{11}$$

with initial condition corresponding to constant solute concentration (C_{ini}) in all segments:

$$C = C_{ini}\ , \quad t = 0,\ r = r_i,\ 1 \leq i \leq n. \tag{12}$$

Both boundary conditions are of the flux type, according to

$$-D(\theta)\frac{\partial C}{\partial r}\bigg|_{r=r_i} + qC = F\ , \quad t > 0,\ r_i = \{r_0, r_m\}\,. \tag{13}$$

From the assumed geometry (Figure 2) it follows that the boundary condition at the outer segment corresponds to zero solute flux (q_s):

$$F = 0\ , \qquad\qquad r = r_m. \tag{14}$$

The rate of solute uptake by plant roots can be described by the MM equation, as seen in Chapter **??**. The uptake shape function $\alpha(C)$ can be supposed to follow the concentration dependent MM kinetics, and considering k equal to I_m leads to:

$$\alpha(C) = \frac{C}{K_m + C} \Rightarrow F = \frac{C}{K_m + C}\, I_m \tag{15}$$

where I_m is the maximum uptake rate, C is the solute concentration in soil solution and K_m the Michaelis-Menten constant. I_m can be found experimentally and K_m is to be calibrated as the concentration at which I_m assumes half of its value, being interpreted as the affinity of the plant for the solute.

The boundary condition for solute transport at the root surface (r_0) represents the concentration dependent solute uptake, described by the MM equation 15, with the following assumptions:

- Solute uptake by mass flow of water is only controlled by the transpiration flow, a convective flow that is considered to be passive;
- Plant regulated active uptake corresponds to diffusion;
- Plant demand is equal to the I_m parameter from the MM equation;
- At a soil solution concentration value C_{lim}, the solute flux limits the uptake.

We assume that the plant demand for solute is constant in time. The uptake, however, can be higher or lower than the demand, depending on the concentration in the soil solution at the root surface (Figure 3). If the concentration is bellow a certain limiting value (C_{lim}), the uptake is limited by the solute flux, *i.e.* solute flux can not attend plant demand even with potential values of active uptake. Additionally, solute uptake by mass flow of water can be higher than the plant demand in situations of high transpiration rate and/or for high soil water content. In these cases, we assume that active uptake is zero and all uptake occurs by the passive process. A concentration C_2 (mol) for this situation is calculated. When the concentration is between C_{lim} and C_2, the uptake is equal to the plant demand as a result of the sum of active and passive contributions to the uptake. Assumption 1 states that passive uptake is not controlled by any physiological plant mechanisms and, in order to optimize the use of metabolic energy, active uptake is regulated in such way that it works as a complementary mechanism of extraction to achieve plant demand (Assumption 2). This results in a lower active uptake contribution than that of its potential value. However, the effect of the solute concentration inside the plant on solute uptake and plant demand is not considered in the model. Consequently, a scenario for which the demand is reduced due to an excess of solute concentration in the plant is not considered. This might, in certain situations, lead to an overestimated prediction of uptake.

A piecewise non-linear uptake function that considers these explicit boundary conditions was formulated as:

$$F = \begin{cases} \dfrac{I_m C_0}{K_m + C_0} + q_0 C_0, & \text{if } C_0 < C_{lim} \quad (16) \\ I_m, & \text{if } C_{lim} \leq C_0 \leq C_2 \quad (17) \\ q_0 C_0, & \text{if } C_0 > C_2 \quad (18) \end{cases}$$

with C_{lim} determined by the positive root of

$$C_{lim} = -\frac{K_m \pm \left({K_m}^2 + 4 I_m K_m / q_0\right)^{1/2}}{2}, \tag{19}$$

and C_2 by

$$C_2 = \frac{I_m}{q_0}. \tag{20}$$

The non-linear part of the uptake function resides in Equation 16. As implicit numerical implementations of non-linear functions may result in solutions with stability issues, a linearization of Equation 16 was made, resulting in:

$$F = (\alpha + q_0)\, C_0, \quad \text{if } C_0 < C_{lim} \tag{21}$$

where α (m s^{-1}) and q_0 (m s^{-1}) are the active and passive contributions for the solute uptake slope ($\alpha + q_0$). This linearization is very similar to the one proposed by Tinker and Nye (2000), but does not consider the solute concentration inside the plant. The derivation of Equations 19 to 21 is shown in Appendix **??**.

Finally, the boundary condition at the inner segment refers to the concentration dependent solute flux at the root surface (F, mol m^{-2} d^{-1}) in agreement to Equation and 21 for the non-linear and linear case, respectively. The uptake of each root equals $-F/R$ (mol d^{-1}, the negative sign indicating solute depletion), thus, the condition at the root surface is described by:

$$-D(\theta)\frac{\partial C}{\partial r} + q_0 C_0 = q_{s_0} = -\frac{F}{2\pi r_0 R z}\,, \qquad r = r_0 \tag{22}$$

Numerical implementation

TELL THAT THERE IS ALSO A LINEAR SOLUTION BUT IT WONT BE SHOWN IN THE PAPER. ALSO, THAT IT WONT BE SHOWN THE SOLUTIONS FOR THE COMPARED MODELS. CITE THE THESIS.

In the numerical solution, the combined water and solute movement is simulated iteratively. In a first step, the water movement towards the root is simulated, assuming salt concentrations from the previous time step. In a second step, the salt contents per segment are updated and new values for the osmotic head in all segments are calculated. The first step is then repeated with updated values for the osmotic heads. This process is repeated until the pressure head values and osmotic head values between iterations converge. Flowcharts containing the algorithm structure are shown in the Appendix **??**.

The implicit numerical discretization of Equation 11 yields:

$$\begin{aligned}
&\theta_i^{j+1} C_i^{j+1} - \theta_i^j C_i^j = \frac{\Delta t}{2 r_i \Delta r_i} \times \\
&\left\{ \frac{r_{i-1/2}}{r_i - r_{i-1}} \left[q_{i-1/2} (C_{i-1}^{j+1} \Delta r_i + C_i^{j+1} \Delta r_{i-1}) - 2 D_{i-1/2}^{j+1} (C_i^{j+1} - C_{i-1}^{j+1}) \right] - \right. \\
&\left. \frac{r_{i+1/2}}{r_{i+1} - r_i} \left[q_{i+1/2} (C_i^{j+1} \Delta r_{i+1} + C_{i+1}^{j+1} \Delta r_i) - 2 D_{i+1/2}^{j+1} (C_{i+1}^{j+1} - C_i^{j+1}) \right] \right\}
\end{aligned} \tag{23}$$

Applying equation 23 to each segment, the concentrations for the next time step C_i^{j+1} (mol m^{-3}) are obtained by solving the following tridiagonal matrix:

$$\begin{bmatrix}
b_1 & c_1 & & & & \\
a_2 & b_2 & c_2 & & & \\
 & a_3 & b_3 & c_3 & & \\
 & & \ddots & \ddots & \ddots & \\
 & & & a_{n-1} & b_{n-1} & c_{n-1} \\
 & & & & a_n & b_n
\end{bmatrix}
\begin{bmatrix}
C_1^{j+1} \\ C_2^{j+1} \\ C_3^{j+1} \\ \vdots \\ C_{n-1}^{j+1} \\ C_n^{j+1}
\end{bmatrix}
=
\begin{bmatrix}
f_1 \\ f_2 \\ f_3 \\ \vdots \\ f_{n-1} \\ f_n
\end{bmatrix} \tag{24}$$

with f_i(mol m^{-2}) defined as

$$f_i = r_i \theta_i^j C_i^j \tag{25}$$

and a_i (m), b_i (m) and c_i (m) defined for the respective segments as described in the following.

1. The intermediate nodes **($i = 2$ to $i = n-1$)**

Rearrangement of Equation 23 to 24 results in the coefficients:

$$a_i = -\frac{r_{i-1/2}(2D^{j+1}_{i-1/2} + q_{i-1/2}\Delta r_i)\Delta t}{2(r_i - r_{i-1})\Delta r_i} \tag{26}$$

$$b_i = r_i\theta^{j+1}_i + \frac{\Delta t}{2\Delta r_i}\left[\begin{array}{l} \frac{r_{i-1/2}}{(r_i - r_{i-1})}(2D^{j+1}_{i-1/2} - q_{i-1/2}\Delta r_{i-1}) + \\ \frac{r_{i+1/2}}{(r_{i+1} - r_i)}(2D^{j+1}_{i+1/2} + q_{i+1/2}\Delta r_{i+1}) \end{array}\right] \tag{27}$$

$$c_i = -\frac{r_{i+1/2}\Delta t}{2\Delta r_i(r_{i+1} - r_i)}(2D^{j+1}_{i+1/2} - q_{i+1/2}\Delta r_i) \tag{28}$$

2. The outer boundary **($i = n$)**

Applying boundary condition of zero solute flux, the third and fourth terms from the right hand side of Equation 23 are equal to zero. Thus, the solute balance for this segment is written as:

$$\theta^{j+1}_n C^{j+1}_n - \theta^j_n C^j_n = \frac{\Delta t}{2r_n\Delta r_n}\times \left\{\frac{r_{n-1/2}}{r_n - r_{n-1}}\left[\begin{array}{l} q_{n-1/2}(C^{j+1}_{n-1}\Delta r_n + C^{j+1}_n\Delta r_{n-1}) - \\ 2D^{j+1}_{n-1/2}(C^{j+1}_n - C^{j+1}_{n-1}) \end{array}\right]\right\} \tag{29}$$

Rearrangement of Equation 29 to 24 results in the coefficients:

$$a_n = -\frac{r_{n-1/2}(2D^{j+1}_{n-1/2} + q_{n-1/2}\Delta r_n)\Delta t}{2(r_n - r_{n-1})\Delta r_n} \tag{30}$$

$$b_n = r_n\theta^{j+1}_n + \frac{\Delta t}{2\Delta r_n}\left[\frac{r_{n-1/2}}{r_n - r_{n-1}}(2D^{j+1}_{n-1/2} + q_{n-1/2}\Delta r_{n-1})\right] \tag{31}$$

3. The inner boundary **($i = 1$)**

(a) For $\boldsymbol{C < C_{lim}}$

Applying boundary conditions of non-linear concentration dependent solute flux, the first and second term of the right-hand side of Equation 23 become $-\left(\frac{I_m}{2\pi r_0 Rz(K_m + C^{j+1}_1)} + q_0\right)C^{j+1}_1\Delta r_1$:

$$\theta^{j+1}_1 C^{j+1}_1 - \theta^j_1 C^j_1 = \frac{\Delta t}{2r_1\Delta r_1}\times \left\{\begin{array}{l} \frac{r_{1-1/2}}{r_1 - r_0}\left[-\left(\frac{I_m}{2\pi r_0 Rz(K_m + C^{j+1}_1)} + q_0\right)\right]C^{j+1}_1\Delta r_1 - \\ \frac{r_{1+1/2}}{r_2 - r_1}\left[\begin{array}{l} q_{1+1/2}(C^{j+1}_1\Delta r_2 + C^{j+1}_2\Delta r_1) - \\ 2D^{j+1}_{1+1/2}(C^{j+1}_2 - C^{j+1}_1) \end{array}\right] \end{array}\right\} \tag{32}$$

Rearrangement of Equation 32 to 24 results in the following coefficients:

$$b_1 = r_1\theta^{j+1}_1 + \frac{\Delta t}{2\Delta r_1}\left[\begin{array}{l} \frac{r_{1+1/2}}{(r_2 - r_1)}(2D^{j+1}_{1+1/2} + q_{i+1/2}\Delta r_2) + \\ \frac{r_{1-1/2}}{r_1 - r_0}\left(\frac{I_m}{2\pi r_0 Rz(K_m + C^{j+1}_1)} + q_0\right)\Delta r_1 \end{array}\right] \tag{33}$$

$$c_1 = -\frac{r_{1+1/2}\Delta t}{2\Delta r_1(r_2 - r_1)}(2D^{j+1}_{1+1/2} - q_{1+1/2}\Delta r_1) \tag{34}$$

(b) For $\boldsymbol{C_{lim} < C < C_2}$

The constant uptake solution is based on the model proposed by De Willigen and Van Noordwijk (1994). The numerical discretization takes into consideration Equation 23, whereas the intermediate nodes are analogous to Equations 26 to 28. The boundary condition at the root surface (Equation 22) corresponds to constant solute flux:

$$q_{s0} = -\frac{I_m}{2\pi r_0 Rz}. \tag{35}$$

Applying boundary conditions of constant solute flux, the first and second term of the right-hand side of Equation 23 become $-\frac{I_m}{2\pi r_0 Rz}\Delta r_1$ for $C > 0$:

$$\theta_1^{j+1}C_1^{j+1} - \theta_1^j C_1^j = \frac{\Delta t}{2r_1\Delta r_1}\times \left\{ \begin{array}{l} \frac{r_{1-1/2}}{r_1 - r_0}\left(-\frac{I_m}{2\pi r_0 Rz}\right)\Delta r_1 - \\ \frac{r_{1+1/2}}{r_2 - r_1}\left[\begin{array}{l} q_{1+1/2}(C_1^{j+1}\Delta r_2 + C_2^{j+1}\Delta r_1) - \\ 2D_{1+1/2}^{j+1}(C_2^{j+1} - C_1^{j+1}) \end{array} \right] \end{array} \right\} \tag{36}$$

When $C = 0$ the solute flux is set to zero and equation 36 reduces to Equation 41. Introduction of Equation 36 in the tridiagonal matrix 24 results in the following coefficients:

$$b_1 = r_1\theta_1^{j+1} + \frac{\Delta t}{2\Delta r_1}\left[\frac{r_{1+1/2}}{(r_2 - r_1)}(2D_{1+1/2}^{j+1} + q_{1+1/2}\Delta r_2)\right] \tag{37}$$

$$c_1 = -\frac{r_{1+1/2}\Delta t}{2\Delta r_1(r_2 - r_1)}(2D_{1+1/2}^{j+1} - q_{1+1/2}\Delta r_1) \tag{38}$$

And the f coefficient changes to:

$$f_1 = r_1\theta_1^j C_1^j - \frac{r_{1-1/2}}{r_1 - r_0} I_m \frac{\Delta t}{4\pi r_0 Rz} \tag{39}$$

(c) For $\boldsymbol{C = 0}$

When $C = 0$ the solute flux is set to zero and the equation is equal to Equation 41 (zero uptake). The zero uptake solution is based on the model proposed by De Jong van Lier et al. (2009). The numerical discretization is according to Equation 23 and the intermediate nodes are analogous to Equations 26 to 28. The only difference is the boundary at the root surface (Equation 22), which is of zero solute flux:

$$q_{s0} = 0 \tag{40}$$

Applying boundary condition of zero solute flux, the first and second term of the right-hand side of Equation 23 are equal to zero:

$$\theta_1^{j+1}C_1^{j+1} - \theta_1^j C_1^j = \frac{\Delta t}{2r_1\Delta r_1}\times \left\{ \frac{r_{1+1/2}}{r_2 - r_1}\left[\begin{array}{l} -q_{1+1/2}(C_1^{j+1}\Delta r_2 + C_2^{j+1}\Delta r_1) + \\ 2D_{1+1/2}^{j+1}(C_2^{j+1} - C_1^{j+1}) \end{array} \right] \right\} \tag{41}$$

Introduction of Equation 41 in the tridiagonal matrix 24 results in the following coefficients:

$$b_1 = r_1\theta_1^{j+1} + \frac{\Delta t}{2\Delta r_1}\left[\frac{r_{1+1/2}}{(r_2 - r_1)}(2D_{1+1/2}^{j+1} + q_{1+1/2}\Delta r_2)\right] \tag{42}$$

$$c_1 = -\frac{r_{1+1/2}\Delta t}{2\Delta r_1(r_2 - r_1)}(2D_{1+1/2}^{j+1} - q_{1+1/2}\Delta r_1) \tag{43}$$

Simulation Scenarios

The simulations were performed using the hydraulic parameters from the Dutch Staring series Wösten et al. (2001) for three different soils types, as listed in Table 1. The general system parameters for the different scenarios are listed in Table 2 and values for the Michaelis-Menten (MM) parameters in Table 4. Values of root length density, initial solute concentration, relative transpiration, soil type, and ion species were chosen at several values, composing eight distinct scenarios as listed in Table **??**. Scenario 1 was considered as default, the other scenarios derive from scenario 1 by changing only one input parameter. In this way, the effect of variation in soil hydraulic properties is exemplified by scenarios 1, 6 and 7; root length density by scenarios 1, 4 and 5; initial solute concentration by scenarios 1 and 3; and potential transpiration by scenarios 1 and 2.

Table 2: System parameters used in simulations scenarios

Description	Symbol	Scenario description	Value	Unit
Root radius	r_0		0.5	mm
Root depth	z		20	cm
Limiting root potential	h_{lim}		-150	m
Root density	R	Low root density Medium root density High root densit	0.01 0.1 1	cm cm^{-3}
Half distance between roots	r_m	Low root density Medium root density High root densit	56.5 17.8 5.65	mm
Potential transpiration rate	T_p	Low High	3 6	mm d^{-1}
Initial solute concentration in bulk soil	C_{ini}	Low High	1 10	mol m^{-3}
Initial pressure head	h_{ini}		-1	m
Diffusion coefficient in water	$D_{m,w}$		$1.98 \cdot 10^{-9}$	m^2 s^{-1}
Dispersivity	τ		0.0005	m
Soil type		Sand Clay Loam	Table 1	

Table 3: Michaelis-Menten parameters for some solutes

Solute	I_m mol m^{-2} s^{-1}	K_m mol m^{-3}
NO_3^-	10^{-5}	0.05
K^+	$2 \cdot 10^{-6}$	0.025
$H_2PO_4^-$	10^{-6}	0.005
Cd^{2+}	10^{-6}	1

The default values of Δr_{min}, Δr_{max} and S in Equation 6 were 10^{-5} m, 5 10^{-4} m and 0.5, resulting in 22, 68 and 213 segments for the high, medium and low root density simulations, respectively. To guarantee complete convergence for the non-linear model, a time step of 0.01 s was used when $C_0 < C_{lim}$. Parameters h_{ini} and C_{ini} were chosen such that the plant is in a no stress condition ($T_r = 1$). All simulation scenarios ended when $T_r \leq 0.001$, at that point considering water uptake to be negligible.

Analysis of linear and non-linear approaches

To analyze the differences between the two proposed models (linear and non-linear solutions), the relative differences in the predicted concentrations (δ_C) and accumulated uptake (δ_{Ac}), for both models, were calculated as follows:

Table 4: Simulation scenarios

Scenario	R	C_{ini}	T_p	Soil	Ion
1	M	H	H	Loam	K^+
2	M	H	L	Loam	K^+
3	M	L	H	Loam	K^+
4	H	H	H	Loam	K^+
5	L	H	H	Loam	K^+
6	M	H	H	Sand	K^+
7	M	H	H	Clay	K^+
8	M	H	H	Loam	NO_3^-

$$\delta_C = \frac{\sum_{x=1}^{x_{end}} CL_x - CNL_x}{\sum_{x=1}^{x_{end}} CL_x} \tag{44}$$

$$\delta_{Ac} = \frac{\sum_{t=1}^{t_{end}} AcL_t - AcNL_t}{\sum_{t=1}^{t_{end}} AcL_t} \tag{45}$$

(46)

where CL_x and CNL_x, are the solute concentration in soil water, and AcL_t and $AcNL_t$ the accumulated uptake, for LU and NLU, respectively. x can be the time (t) or the distance from the axial center (r). The relative difference between three outputs was computed: two relative to time – concentration at the root surface $C_0(t)$ and accumulated solute uptake $Ac(t)$ – and one relative to radial distance – concentration $C(r)$.

NLU solution uses the non-linear MM equation and, due to an additional iterative process in the numerical implementation, more time is needed to compute the results when compared with the linear solution LU. It is also susceptible to numerical stability issues, depending on selected time and space steps. On the other hand, LU is a simplified version of the MM equation in a way that the solute uptake rate for $C_0 < C_{lim}$ is always smaller than that of the original non-linear equation. It has no stability problems and needs less computational time because it is less sensitive to space and time steps. In a first analysis, the objective was to check if the difference in the results generated by the linearization of the MM equation is sufficiently large to be properly analyzed. To do so, four different scenarios were chosen (scenarios 1 to 4 as listed in Table **??**).

Sensitivity analysis

The relative partial sensitivity η de Jong van Lier et al. (2015) of model predictions Y as a function of the respective parameter value P was calculated as

$$\eta = \frac{dY/Y}{dP/P} \tag{47}$$

where P is the default value of the parameter, dP is the in(de)crement applied to P, Y is the output of a selected predicted variable and dY is the variation over Y when applied the new parameter value $P \pm dP$.

To determine the sensitivity of the model to an input parameter, the magnitude of its derivative in respect of the model result is calculated. If this derivative is close to zero, the model has a low sensitivity to the respective parameter. The higher the derivative, the higher is the sensitivity and, therefore, the higher is the precision required when determining that parameter. By making a relative analysis like in Equation 47, the sensitivity for distinct parameters can be compared.

To determine the sensitivity, a dP/P of 0.01 (1%) was used for the following selected parameters: a) MM parameters I_m, K_m; and b) soil hydraulic parameters α, n, λ, K_s, θ_r and θ_s. The analyzed predicted

variables (Y) were: time to completion of simulation t_{end}, osmotic head at completion of simulation h_π, pressure head at completion of simulation h, average osmotic head in the soil profile at completion of simulation $\overline{h_\pi}$, average pressure head in soil profile at completion of simulation $\overline{h}$ and accumulated uptake at completion of simulation Ac.

References

Michael A Celia, Efthimios T Bouloutas, and Rebecca L Zarba. A general mass-conservative numerical solution for the unsaturated flow equation. *Water resources research*, 26(7):1483–1496, 1990.

Quirijn De Jong van Lier, Klaas Metselaar, and Jos C. Van Dam. Root water extraction and limiting soil hydraulic conditions estimated by numerical simulation. *Vadose Zone Journal*, 5(4):1264–1277, 2006.

Quirijn De Jong van Lier, Jos C. Van Dam, and Klaas Metselaar. Root water extraction under combined water and osmotic stress. *Soil Science Society of America Journal*, 73(3):862–875, 2009.

Quirijn de Jong van Lier, Ole Wendroth, and Jos C. van Dam. Prediction of winter wheat yield with the swap model using pedotransfer functions: An evaluation of sensitivity, parameterization and prediction accuracy. *Agricultural Water Management*, 154(1):29–42, 2015.

Peter De Willigen and Meine Van Noordwijk. Mass flow and diffusion of nutrients to a root with constant or zero-sink uptake i. constant uptake. *Soil science*, 157(3):162–170, 1994.

P.B. Tinker and P.H. Nye. *Solute Movement in the Rhizosphere*. Topics in sustainable agronomy. Oxford University Press, 2000.

Jos C Van Dam and Reinder A Feddes. Numerical simulation of infiltration, evaporation and shallow groundwater levels with the richards equation. *Journal of Hydrology*, 233(1):72–85, 2000.

M Th Van Genuchten. A closed-form equation for predicting the hydraulic conductivity of unsaturated soils. *Soil science society of America journal*, 44(5):892–898, 1980.

J H M Wösten, G J Veerman, W J M De Groot, and J Stolte. Waterretentie-en doorlatendheidskarakteristieken van boven-en ondergronden in nederland: de staringsreeks. 2001.

Figures

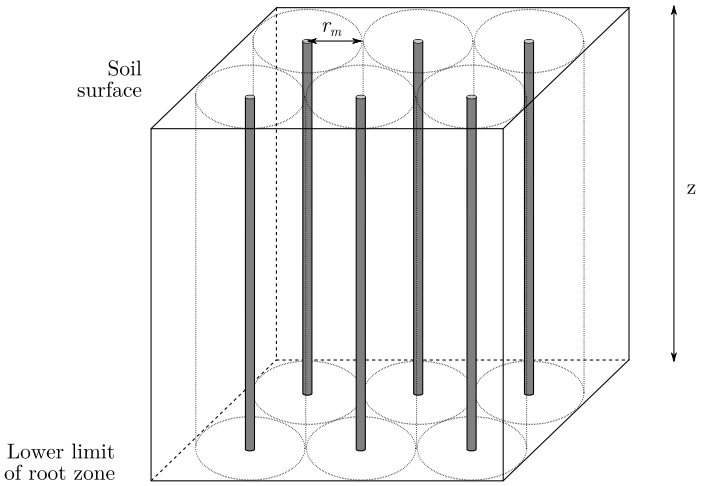

Figure 1: Schematic representation of the spatial distribution of roots in the root zone

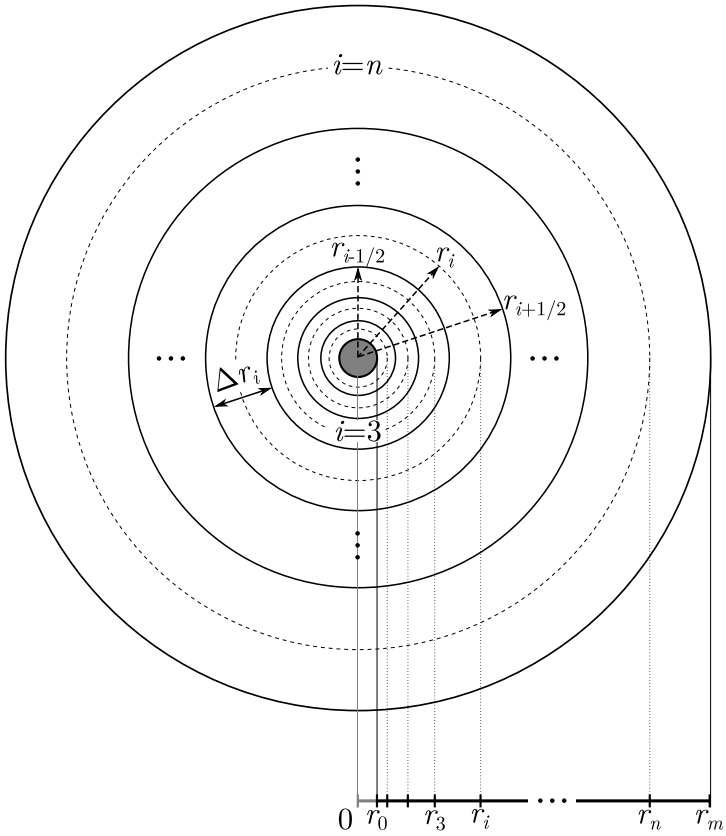

Figure 2: Schematic representation of the discretized domain considered in the model. Δr is the variable segment size, increasing with the distance from the root surface (r_0) to the half-distance between roots (r_m), and n is the number of segments

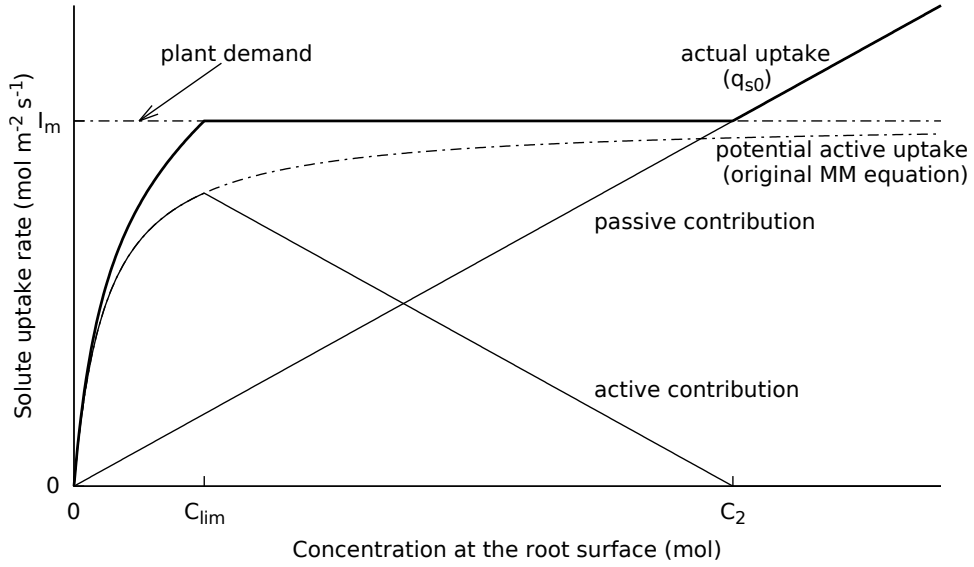

Figure 3: Solute uptake piecewise equation from MM equation 15 with boundary conditions. The bold line represents the actual uptake, thin lines represent active and passive contributions to the actual uptake, and dotted lines represent the plant demand and the potential active uptake